Directional anisotropy of diffuse solar irradiance: impact assessment on the solar transmittance of common glazings

Juan M. Rodríguez-Muñoz[1], Gerardo Vitale[1], Italo Bove[2], Gonzalo Abal[1,2]
[1]Laboratorio de Energía Solar, Departamento de Física del Litoral,
CENUR Litoral Norte, Universidad de la República, Uruguay
[2]Laboratorio de Energía Solar, Instituto de Física, Facultad de Ingeniería,
Universidad de la República, Uruguay

Abstract

The solar transmittance of transparent glazings is a key factor in determining the solar gain and thermal balance of a building. The transmittance calculation must be made separately for the beam and diffuse components of the incident solar irradiance. Most simulation software uses an isotropic distribution for diffuse irradiance, approximation that can be inaccurate under clear or partially cloudy skies. An anisotropic distribution of diffuse irradiance is implemented in this work, its diffuse transmittance is evaluated for real sky conditions and compare against experimental data. The results show that the anisotropic model does not offer significant advantages over the isotropic one.

Highlights

- The accuracy of the isotropic assumption for estimating the diffuse irradiance transmitted by a glazing is investigated.
- An anisotropic model is implemented providing a more precise model for all sky conditions.
- Both modelled approaches are compared against experimental data, both in terms of solar transmittance and solar gain.
- These results aid in estimating the accuracy of the isotropic assumption for diffuse irradiance used by most building simulation software.

Introduction

Solar gains through semitransparent glazings play an important role in the energy simulation of buildings. Usually, a two-step procedure is implemented in which (i) the solar irradiance incident on the different glazings is calculated, taking into account the location and their orientations and (ii) the solar transmittance of the glazing is estimated. The product of both quantities produces solar irradiance transmitted through each glazing in the 0.3 - 3 μm range. This calculations are done separately for each component (beam, diffuse) of solar irradiance.

The beam (or directional) transmittance of a glazing can be adequately modelled using physical or empirical models (Vitale et al., 2019). The diffuse transmittance is usually computed assuming an isotropic distribution of the diffuse irradiance incident on the glazing and integrating over the visible part of the sky (Brandemuehl and Beckman, 1980). This geometrical calculation is a reasonable approximation under cloudy conditions, but it may be inadequate under partially cloudy or clear skies, particularly if the Sun disc is visible. Circumsolar irradiance (forward scattered diffuse irradiance which reaches the ground from the angular region around the apparent solar disc) is a source of anisotropy as are beam reflections from clouds or nearby reflective surfaces.

Several empirical functions have been proposed that attempt to describe the diffuse irradiance anisotropical distribution under different sky conditions (Perez et al., 1990; Brunger and Hooper, 1993a; Igawa et al., 2004). However, the effects of anisotropy on building performance simulation has not been evaluated yet and these anisotropic models are not incorporated into building simulation programs. In this work we use one of the anisotropic distribution (Brunger and Hooper, 1993a) to compute the diffuse solar transmittance of a common glazing, and compare the results with those obtained using the standard isotropic approximation. In order to assess both models, experimental data from two different set-ups using common 6 mm clear (float) glass are used: an horizontal glazing and a vertical glazing oriented towards the equator. The resulting solar gains are also compared in order to provide information on the accuracy impact of using the isotropic approximation.

This work is organized as follows. The next Section describes the model used for estimating the beam and diffuse solar transmittance across glazings. Next, the experiments, the collected transmittance data and its quality control procedures are described. The third Section describes the methodology and the results obtained and the final Section summarizes the conclusions.

Glazing transmittance model

The solar transmittance of a semi-transparent glazing, τ_g, is defined as the fraction of the incident (G_i) and transmited (G_t) global hemispherical solar irradiances,

$$\tau_g = \frac{G_t}{G_i}, \tag{1}$$

which extend over the incident solar spectrum (0.3 to 3 μm). The transmittance of a planar glazing is calculated differently for the beam and diffuse components of global solar irradiance. For the general case of a non-horizontal glazing, the irradiance reflected from surrounding surfaces (G_r) must also be taken into account, so that $G_i = G_{bi} + G_{di} + G_{ri}$, where $G_{bi} = G_b \cos\theta$ is the beam irradiance across the surface and θ is incidence angle of the solar beam. For this paper, the usual assumption that the ground is the only relevant reflective surface and that it is a perfect diffuser of reflectivity ρ_g matches our experimental conditions and it is thus adopted. The total transmittance, Eq. (1), can be expressed as a weighted average of the transmittances of the beam (τ_b), diffuse (τ_d) and reflected (τ_r) components of the incident irradiance,

$$\tau_g = \tau_b \frac{G_{bi}}{G_i} + \tau_d \frac{G_{di}}{G_i} + \tau_r \frac{G_{ri}}{G_i}. \tag{2}$$

Usually, the incident diffuse irradiances is assumed to be isotropically distributed and only the first term in this expression has a directional dependence. In order to calculate the solar radiation transmitted by the glazing, Building Performance Simulation Programs (BPSP) can be used. These programs calculate each component of solar radiation on the glazing's plane and their respective solar transmittances. Generally, the meteorological files used in BPSP's provide solar irradiation (global and diffuse components) on a horizontal plane. A transposition model is internally used to convert these magnitudes to the corresponding ones on the glazing's plane. These models, when non-trivial, account for the anisotropical distribution of diffuse irradiance in the sky. EnergyPlus, one of the most widely used BPSP around the world, uses the transposition model of Perez et al. (1990), one of the best performing (for most locations) transposition models available (Yang, 2016). In the next sub-sections we briefly describe the models used for calculating the beam and diffuse transmittances of a glazing.

Beam transmittance

Beam transmittance is directional and it can be modeled successfully by physical or phenomenological models Vitale et al. (2019). In this work we consider the physical model adequate for uniform semi-transparent glazings, such as float glass. This is based on Snell's law and the Fresnel relations as described in Duffie and Beckman (2006).

The beam transmittance is approximated as the product $\tau_b = \tau_a \times \tau'_r$, where τ_a takes into account the losses due to internal absorption in the glazing and τ'_r accounts for reflections in the glazing.

The absorption transmittance results from the Lambert-Beer-Bouguer law,

$$\tau_a = \exp\left(\frac{-kL}{\cos\theta'}\right) \quad \text{with} \quad \theta' = \arcsin\left(\frac{\sin\theta}{n}\right), \tag{3}$$

where L is the thickness of the glazing (m), k is the optical extinction coefficient (m^{-1}), θ is the beam incident angle on the glazing's surface, θ' is the angle of the refracted beam in the glazing and n es the index of refraction of the glazing.

The reflection transmittance, τ'_r, for unpolarized sunlight is expressed as

$$\tau'_r = \frac{1}{2}\left(\frac{1-r_\parallel}{1+r_\parallel} + \frac{1-r_\perp}{1+r_\perp}\right), \tag{4}$$

with the reflectances for the parallel and perpendicular polarization components obtained from the Fresnel relations, $r_\parallel = [\tan(\theta'-\theta)/\tan(\theta'+\theta)]^2$ and $r_\perp = [\sin(\theta'-\theta)/\sin(\theta'+\theta)]^2$.

Finally, accounting for multiple reflections within the glazing, the directional transmittance from the model can be expressed as

$$\tau_b = \frac{\tau_a}{2}\left[\frac{(1-r_\parallel)^2}{1-(r_\parallel\tau_a)^2} + \frac{(1-r_\perp)^2}{1-(r_\perp\tau_a)^2}\right]. \tag{5}$$

In sum, τ_b is determined by the properties of the glazing (kL and n) and the beam incidence angle θ.

Diffuse transmittance

As mentioned, most BPSP's calculate τ_d and τ_r assuming an isotropic behavior for the diffuse irradiances (incident from the visible sky and reflected from the ground). In this case, both transmittances, τ_d and τ_r, are independent of the incidence angle (for a given glazing and orientation). In this work a more general model is proposed for the calculation of τ_d, which uses a more realistic distribution for diffuse solar radiation from the sky, L_p.

Anisotropic effects in diffuse irradiance are introduced by considering the sky angular radiance, $L_p(\varphi,\sigma)$, describes the flux of radiant energy per unit solid angle incoming from each sky direction (φ,σ), including circumsolar radiation but excluding the direct beam (Rodríguez-Muñoz et al., 2021). So, the diffuse irradiance reaching the glazing's surface is

$$G_{di} = \int_\Lambda L_p(\varphi,\sigma)\,\cos\theta\, d\Omega, \tag{6}$$

with $d\Omega = \sin\varphi\, d\varphi\, d\sigma$ and Λ describing the portion of the sky viewed from the glazing's surface. A similar expression for the transmitted diffuse irradiance

by the glazing can be obtained by weighting each direction by the direct transmittance τ_b,

$$G_{dt} = \int_{\Lambda} \tau_b(\theta)\, L_p(\varphi,\sigma)\, \cos\theta\, d\Omega. \tag{7}$$

The sky diffuse transmittance, $\tau_d = G_{dt}/G_{di}$, can be expressed, for an arbitrary glazing's surface orientation (γ,β), as follows (Brandemuehl and Beckman, 1980)

$$\begin{aligned}\tau_d =& \frac{\int_{\gamma-\frac{\pi}{2}}^{\gamma+\frac{\pi}{2}} \int_0^{\frac{\pi}{2}} L_p(\varphi,\sigma)\tau_b(\theta)\cos\theta d\Omega}{\int_{\gamma-\frac{\pi}{2}}^{\gamma+\frac{\pi}{2}} L_p(\varphi,\sigma)\cos\theta d\Omega} \\ &+ \frac{\int_{\gamma+\frac{\pi}{2}}^{\gamma+\frac{3\pi}{2}} \int_0^{\zeta} L_p(\varphi,\sigma)\tau_b(\theta)\cos\theta d\Omega}{\int_{\gamma+\frac{\pi}{2}}^{\gamma+\frac{3\pi}{2}} \int_0^{\zeta} L_p(\varphi,\sigma)\cos\theta d\Omega},\end{aligned} \tag{8}$$

with $\zeta = \arctan\left[(-\tan\beta\cos\gamma)^{-1}\right]$. Except for a few special cases, this expression must be numerically evaluated for each surface orientation.

For an isotropic distribution of diffuse irradiance, the usual assumption in BPSP's, the sky angular radiance is independent of direction and takes the value $L_p = G_{dh}/(2\pi)$, in terms of G_{dh}, the diffuse solar irradiance incident on a horizontal plane. In this case, the surface integral in Eq. (8) is independent of surface orientation. In the anisotropic case, the integral is complex because the sky angular radiance is a function of the sky condition (cloudiness) and the sun's position. Brunger and Hooper (1993a) simplified this problem by finding an expression[1] for the sky radiance that explicitly depends on the Sun's position,

$$L_p(\varphi,\sigma) = G_{dh}\left[\frac{a_0 + a_1\cos\theta + a_2\, e^{-a_3\psi}}{\pi\,(a_0 + 2a_1/3) + 2a_2\, I(\varphi_z)}\right], \tag{9}$$

with

$$\begin{aligned} I(\varphi_z) =& \left[\frac{1+e^{-a_3\pi/3}}{1+a_3^2}\right] \\ &\times \left[\pi - \left(1 - \frac{2}{\pi a_3}\cdot\frac{1-e^{-a_3\pi}}{1+e^{-a_3\pi/2}}\right)\right. \\ &\left.\times\,(2\varphi_z\sin\varphi_z - 0.02\,\pi\,\sin(2\varphi_z))\right]. \end{aligned} \tag{10}$$

The Sun's position dependence appears through ψ, the angle subtended between a given sky element (φ,σ) and the Sun's position (φ_z,σ_z). The dependence on the sky conditions is introduced by the coefficients a_i which are discrete functions of the clearness index, defined as $k_t = G_h/G_{0h}$, with G_h the global irradiance on a horizontal plane and G_{0h} is the corresponding irradiance at the top of the atmosphere, and the diffuse fraction $f_d = G_{dh}/G_h$. The coefficients a_i in Eq. (9), where originally determined in Brunger and Hooper (1993a) by adjusting the model (using non-linear regression) to one year of data from sky scans made in Toronto, Canada (latitude $\phi = 43.67°$). These are given for a matrix of 9×9 bins in (k_t, f_d) space, describing all sky conditions. When this distribution is plotted for different sky conditions, the anisotropic effects are greater for clear and partly cloudy skies. For completely cloudy sky conditions the distribution approaches the isotropic, as expected. Although other sky distributions have been proposed (Moon and Spencer, 1942; Perez et al., 1990; Igawa et al., 2004), the radiance distribution of Brunger and Hooper (1993a) is used in this work due to its balance between simplicity and performance (Igawa et al., 2004; Rodríguez-Muñoz et al., 2021).

It remains to consider the reflected component of incident irradiance. Since the only reflecting surface is assumed to be the ground and it is modelled as a perfect diffuse reflector, this irradiance is isotropically distributed in the solid angle spanned by the ground. Thus, the reflected transmittance τ_r can be found from,

$$\tau_r = \frac{\int_{-\frac{\pi}{2}}^{\frac{\pi}{2}} \int_0^{\beta} \tau_b(\theta)\cos\theta d\Omega}{\int_{-\frac{\pi}{2}}^{\frac{\pi}{2}} \int_0^{\beta} \cos\theta d\Omega}. \tag{11}$$

For a fixed glazing and orientation, this expression evaluates to a constant contribution.

Data and quality control

Experimental set-up

In order to assess the performance of the previous models, two experimental set-ups were implemented at the Solar Energy Laboratory (Salto, Uruguay, latitude = 31.28° S, longitude = 57.92° W, altitude = 56 m above sea level). The transmittance of two samples of common float glass was measured, one mounted on a horizontal plane and the other on a vertical plane facing the equator.

The experimental setup for measurements in the horizontal plane is shown in Figure 1. Two Kipp & Zonen CMP10 pyranometers were used, one behind the glazing and the other in front: measuring G_t and G_i, respectively. This glazing had a thickness of $L = 6.15\,\text{mm} \pm 0.05\,\text{mm}$. For the vertical plane, two LI-COR LI-200R photovoltaic solar radiometers were used, one behind the glazing and the other in front, as shown in the Figure 2. These instruments have a fast time response and are less sensitive to changes in their measuring plane, as compared with dome-equipped pyranometers. This glazing had a thickness of $L = 5.90\,\text{mm} \pm 0.05\,\text{mm}$. The air temperatures close to these sensors was recorded to make the corresponding post-processing corrections (Wilbert et al., 2015). In both cases the global transmittance τ_g were calculated using Eq. (1). Additionally, a precision solar tracking system (Kipp & Zonen, SOLYS2) with

[1] Note that the first factor in Eq. (10) originally appeared with an erratum, corrected in Brunger and Hooper (1993b).

two Kipp & Zonen CMP11 pyranometers, one of them shaded by a ball assembly, measure the global and diffuse horizontal irradiances, G_h and G_{d_h}. All these instruments are calibrated every two years following the ISO 9847:1992 standard, against a secondary standard (Kipp & Zonen CMP22) with traceability to the World Radiometric Reference (WRR).

Figure 1: Experimental set up for the horizontal measurements.

Figure 2: Experimental set up for the vertical measurements (facing the equator).

Instantaneous measurements were recorded at one-minute intervals by three different (Fischer-Scientific DT85) data acquisition systems: the first for the horizontal measurements, the second for the vertical measurements and the third for the Solys2 mounted measurements. A one-minute dataset for the solar irradiance variables G_h, G_{dh}, G_i and G_t was assembled for each orientation and then this data was averaged at 10-minute intervals. The measurement period for vertical measurements was extended from 27/05/2016 to 10/12/2018, while horizontal measurements was extended from 29/12/2018 to 04/02/2019.

Quality control

A quality control procedure based on the Baseline Solar Radiation Network (BSRN) recommended filters (McArthur, 2005) was applied to the datasets of both orientations, with some additional filters based of physical boundaries, visual inspection of the data and statistical analysis where applied to the transmittance data.

The first three filters (F1 to F3 in the upper pane of Table 1) are lower and upper bounds for the measured horizontal irradiances, G,

$$b \leq G \leq G_{sc}\, p\, (\cos\theta_z)^a + c, \tag{12}$$

where p, a and c are parameters by inspection of each tested variable (G_h, G_d, G_t). Filter F4 discards low-altitude (α_s) measurements which may be affected by larger cosine errors. F5 is an upper bound for the diffuse fraction, with a 3 % tolerance for experimental errors. F6 removes points of low k_t and low f_d (mostly associated with very low-irradiance measurements under heavy overcast conditions). Filter F7 ($k_t < 1$) excludes a few over-irradiance events, which are rare in 10-min records. Filter F8 is a consistency check for the transmittance measurements, $0 \leq \tau_g \leq 1$. Finally, the F9 filter rejects statistical outliers in transmittance. For different bins in solar the zenith angle, it removes the data points that do not comply with $\|\tau_g - \bar{\tau}_g\| \leq 3\sigma$, where $\bar{\tau}_g$ and σ are the mean and standard deviation of the transmittance measurements in each bin. This filter was applied independently in 5° bins (the calculation of $\bar{\tau}_g$ and σ is done with the data points that pass F1 to F8).

Table 1 shows each filtering condition, the variables affected and the % of the daytime records that are discarded. The last row of this table summarizes the process by giving the % of records that pass all filters. After this procedure, a 2282 10-minute record data set is obtained for the horizontal glazing. Figure 3a shows the filtering result in terms of horizontal transmittance measurements. A similar filtering procedure was used for the vertical measurements (lower pane in Table 1). Filter F6' limits the incidence angle θ on the vertical plane. Finally, 13455 10-minute data records that pass all the filters are obtained. Figure Fig. 3b summarizes the filtering process for this orientation.

Methodology

Two transmittance models were implemented for each orientation, isotropic and anisotropic. Both of them use Eq. (5) for the beam transmittance and differ in the calculation of the diffuse transmittance, Eq. (8). The isotropic model uses $L_p = G_{dh}/2\pi$ and the anisotropic one uses Eqs. (8) and (9) calculating the integral numerically with a resolution of one degree in the integration domain. For the vertical case, the reflected transmittance was calculated from Eq. (11) with $\rho = 0.30$, as the reflectivity of the surrounding ground that best matches the experimental data. In this case, the incident diffuse irradiance G_{di} was

Table 1: Filters applied to the diurnal measurements. For the horizontal data set from 3084 diurnal records, 2282 pass all filters. For the vertical data set, from 48399 diurnal records, 13455 pass all filters. % are expressed in terms of the initial diurnal records.

Filter	condition	variable	% discarded
Horizontal plane			
F1	Eq. (12)	G_h	5.4
F2	Eq. (12)	G_t	6.4
F3	Eq. (12)	G_{dh}	5.5
F4	$\alpha_s > 10°$	all	12.6
F5	$f_d < 1.03$	G_h, G_{dd}	4.3
F6	$k_t < 0.20$ & $f_d < 0.80$	G_h, G_{dh}	9.0
F7	$k_t < 1$	G_h	0.3
F8	$0 \leq \tau_g \leq 1$	G_t, G_i	0.6
F9	$\|\tau_g - \bar{\tau}_g\| \leq 3\sigma$	G_t, G_i	16.7
all	–	all	26.0
Vertical plane			
F1'	Eq. Eq. (12)	G_h	6.2
F2'	Eq. Eq. (12)	G_{dh}	7.6
F3'	Eq. Eq. (12)	G_i	24.0
F4'	Eq. Eq. (12)	G_t	13.5
F5'	$\alpha_s > 10°$	all	14.2
F6'	$\theta < 80°$	G_i, G_t	34.9
F7'	$f_d < 1.03$	G_h, G_{dh}	4.9
F8'	$k_t < 0.20$ & $f_d < 0.80$	G_h, G_{dh}	5.6
F9'	$k_t < 1$	G_h	0.6
F10'	$0 \leq \tau_g \leq 1$	G_i, G_t	7.5
F11'	$\|\tau_g - \bar{\tau}_g\| \leq 3\sigma$	G_t, G_t	42.2
all	–	all	61.3

estimated from the horizontal irradiance, using the transposition model of Perez et al. (1990).

Both glass samples have the same physical properties. A refractive index of 1.53 and an extinction coefficient of 28.9 m^{-1} were used. The first parameter was measured using a red laser with $\lambda = 633\,\mathrm{nm}$ and a precision goniometer and the second one results from a fit to the experimental data minimizing the root mean square error (see next Section).

Performance indicators

The models are evaluated experimental data by using three common metrics, namely, the Mean Bias Deviation (MBD), the Root Mean Square Deviation (RMSD) and the Kolmogorov-Smirnov Integral (KSI). These quantities are defined as follow,

$$\begin{aligned} \mathrm{MBD} &= \frac{1}{n}\sum_{i=1}^{n}(\hat{y}_i - y_i), \\ \mathrm{RMSD} &= \left[\frac{1}{n}\sum_{i=1}^{n}(\hat{y}_i - y_i)^2\right]^{\frac{1}{2}}, \\ \mathrm{KSI} &= \int_0^{y_m} |F(y) - \hat{F}(y)|\, dy, \end{aligned} \tag{13}$$

where y_i stands for the reference (measured) value, $\hat{y}_i$ for the modeled (estimated) value, y_m for the maximum of both sets and F and $\hat{F}$ are the cumulative distribution functions of y_i and $\hat{y}_i$, respectively. This set of indicators has been used successfully in previous works (Vitale et al., 2019; Rodríguez-Muñoz et al., 2021). These metrics are expressed in relative terms

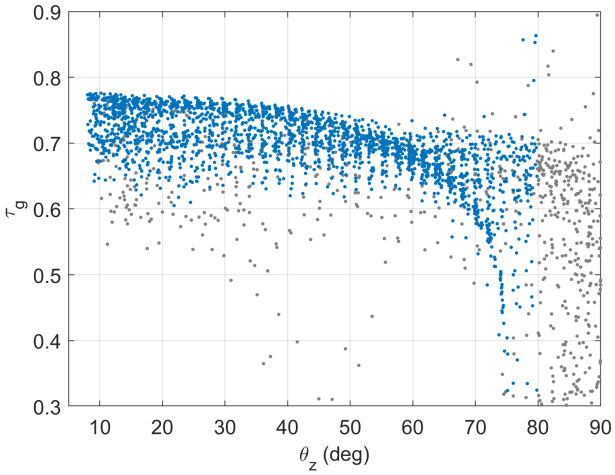

(a) Horizontal measurements.

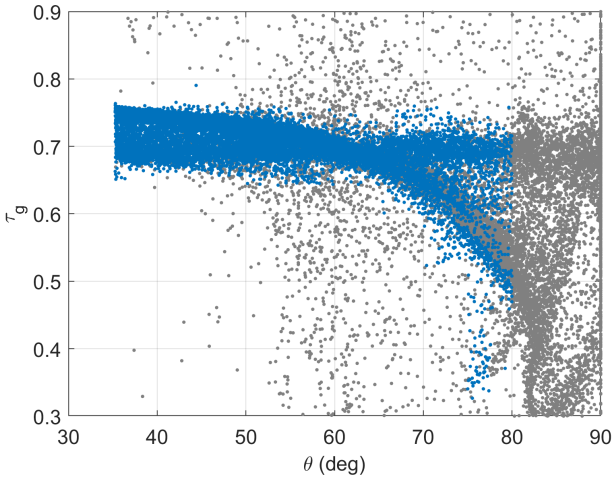

(b) Vertical measurements facing to the equator.

Figure 3: Transmittance measurements as a function of the incidence angle. Raw daytime measurements are in gray, those measurements that pass all filters are in blue.

(rMBD, rRMSD and rKSI) as a percentage of the average measured value.

Since each of them quantifies a different aspect of the comparison between the measured and corrected data sets, it is convenient to define a collective performance indicator as,

$$\mathrm{CPI} = \frac{1}{3}\left(|\mathrm{rMBD}| + \mathrm{rRMSD} + \mathrm{rKSI}\right). \tag{14}$$

This global index, also expressed as a percentage of the average reference value, is used as an indicator for overall model performance. In Gueymard (2014) uses for these and other indicators in the context of solar resource assessment are discussed.

In this work, these indicators were calculated for the entire data set and also for three specific sky conditions by clearness index: clear sky ($k_t > 0.6$), partly cloudy sky ($0.2 < k_t < 0.6$) and overcast sky ($k_t < 0.2$).

Results

Transmittance models' performance

In Table 2, the performance indicators for the transmittance of each glazing (horizontal and vertical orientations) are shown, discriminated by sky condition. The indicators in this table are expressed as a percentage to the average experimental transmittance, $\bar{\tau}_g = 0.689$ (horizontal) and $\bar{\tau}_g = 0.702$ (vertical). The horizontal plane shows positive biases (overestimation) and the vertical plane has negative biases (underestimation), small in both cases. When considering all sky conditions (all data in Table 2), the differences between the isotropic and anisotropic models are very small. The indicators for the anisotropic model are slightly better than those of the isotropic model, except for the mean bias. Since this increase in rMBD is mostly offset by the decline of the other indicators when anisotropy is considered, the CPI remains the same as for the isotropical case.

When the performance is analyzed by sky condition, the improvement from the anisitropic model is associated to clear and partly cloudy conditions. Under cloudy conditions the isotropic model performs best. This is interesting because under cloudy conditions the diffuse distribution is approximately isotropic and the models should have similar performance indicators. This may be due to the fact that the parameters a_i of the function L_p of Brunger and Hooper (1993a) were fitted with very few experimental data in the region $k_t < 0.2$. In some cases, values for a_i had to be extrapolated to be able to include sky conditions within the region $k_t < 0.2$ originally not considered in Brunger and Hooper (1993a). A simple fix for this situation is obtained by considering anisotropy only for $k_t \geq 0.20$ and using the isotropic approximation otherwise. The results of this approach are shown in Table 2 as the "Combined" model which performs slightly better than the isotropic or anisotropic models, with improvements of 3-5% on the combined (CPI) indicator respect to the isotropic results.

The analysis is complemented by Fig. 4, which compare the experimental transmittance data (in blue) and the theoretical data (in red) in terms of transmittance vs. angle of incidence diagrams. Both adequately describe the general trend of the transmittance with respect to the angle of incidence.

Energetic impact on BPSP

In the last Subsection, the ability of the isotropic and anisotropic models (and their combination) to predict the glazing transmittance was evaluated. However, global transmittance estimates are associated to different solar gains, according to $G_t = \tau_g G_i$, so that equal transmittances value may have different impacts in solar gain due to changes in incident irradiance. The overall impact in the energy balance is not easy to estimate, since it will depend on the area and orientations of all glazings among other factors.

A simplified analysis of the impact on energy balance can be done by considering performance indicators in terms of the transmitted irradiances. This is equivalent to weight the metrics in Table 2 by the incident solar irradiance. These performance indicators are shown in Table 3 for all sky conditions. They are expressed in relative terms to the average of measured transmitted solar irradiance: $\bar{G}_t = 343\,\mathrm{W/m^2}$ for the horizontal case and $\bar{G}_t = 265\,\mathrm{W/m^2}$ for the vertical case. For the vertical glazing, two cases are considered: (i) using the measured incident global irradiance and (ii) using the measured horizontal irradiance (global and diffuse) and the Perez et al. (1990) transposition model to estimate the irradiance components on the glazing. This second alternative is included because it is frequently used by building simulation software which mostly uses solar data on a horizontal plane and contributes to the overall uncertainty in solar gain.

As shown in Table 3, in terms of transmitted irradiance the difference between both (isotropic and anisotropic) models is larger, with the anisotropic reducing the combined indicator (CPI) between 12 − 22 % respect to the isotropic value. This is to be expected, because anisotropy matters most under clear sky, when the incident irradiance is largest. When these results are analyzed in terms of different sky conditions, similar results as those obtained in terms of transmittance are obtained, so they are not included. When the transposition model is included as part of the solar gain calculation, (last three rows in Table 3) a considerable decrease in performance is obtained. The improvements due to the anisotropic model are reduced to 3 % in CPI), due to the uncertainty introduced by the transport procedure.

However, it must be noted that in all cases, the performance indicators are similar (or even less) than the estimated typical uncertainty in the measured data. For solar irradiance, typical uncertainties are between 3-5% depending on the quality of the instruments, the incidence angle, temperature and other factors. This leads to a typical uncertainty in measured transmittance of 4-7%. Thus, even if a small improvement is observed with the use of the anisotropic model for incident diffuse irradiance, when considering a balance between complexity and performance, the isotropic model is still the best option for use in BPSP in most situations. The anisotropic model might be relevant for special cases, such as buildings with large glazing to wall ratios on which the Sun has small incidence angles during a significant portion of the time (i.e. equator facing vertical glazings in high latitudes or horizontal glazings in low latitudes).

Table 2: Performance indicators for isotropic and anisotropic model, expressed as a percentage of the average reference transmittance, $\bar{\tau}_g = 0.689$ for the horizontal case and $\bar{\tau}_g = 0.702$ for the vertical case.

Sky condition	Model	Horizontal plane				Vertical plane			
		rRMSD	rMBD	rKSI	CPI	rRMSD	rMBD	rKSI	CPI
all data	Isotropic	7.0	0.8	2.7	5.8	2.9	-1.0	1.4	2.7
	Anisotropic	6.8	1.7	2.7	5.8	2.9	-1.0	1.2	2.7
	Combined	6.6	1.3	2.0	5.5	2.8	-0.9	1.1	2.6
clear sky	Isotropic	5.1	-0.4	1.7	4.1	3.0	-1.4	1.8	3.1
$k_t > 0.6$	Anisotropic	4.8	-0.4	1.5	3.8	2.9	-1.1	1.6	2.9
partly cloudy sky	Isotropic	9.2	1.7	4.0	8.0	2.7	-1.1	1.3	2.6
$0.6 > k_t > 0.2$	Anisotropic	8.7	3.0	3.0	7.8	2.7	-1.1	1.2	2.6
overcast sky	Isotropic	6.0	1.7	3.0	5.6	2.9	0.2	1.3	2.4
$k_t < 0.2$	Anisotropic	7.0	3.6	4.1	7.3	3.2	-0.5	1.2	2.7

Table 3: Performance indicators for the isotropic and anisotropic model in terms of transmitted solar irradiance, expressed as a percentage of average transmitted solar irradiance, $\bar{G}_t = 343\,\mathrm{W/m^2}$ for the horizontal case and $\bar{G}_t = 265\,\mathrm{W/m^2}$ for the vertical case.

Sky condition	Model	Horizontal plane				Vertical plane			
		rRMSD	rMBD	rKSI	CPI	rRMSD	rMBD	rKSI	CPI
all data	Isotropic	3.2	-0.7	1.6	2.9	2.7	-1.4	1.5	2.7
G_i measured	Anisotropic	2.9	0.1	1.1	2.3	2.4	-1.2	1.1	2.4
	Combined	2.9	0.0	1.1	2.3	2.4	-1.2	1.1	2.4
all data	Isotropic	-	-	-	-	8.8	-1.1	2.2	7.0
G_i estimated	Anisotropic	-	-	-	-	8.8	-0.9	2.0	6.8
(Perez et al., 1990)	Combined	-	-	-	-	8.8	-0.8	2.0	6.8

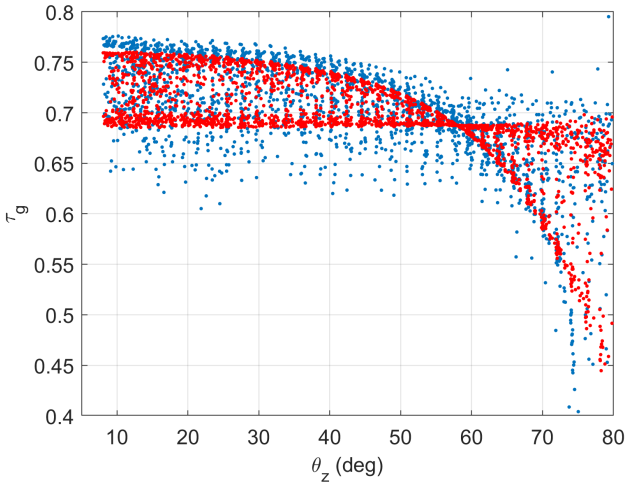

(a) Isotropic model for horizontal case

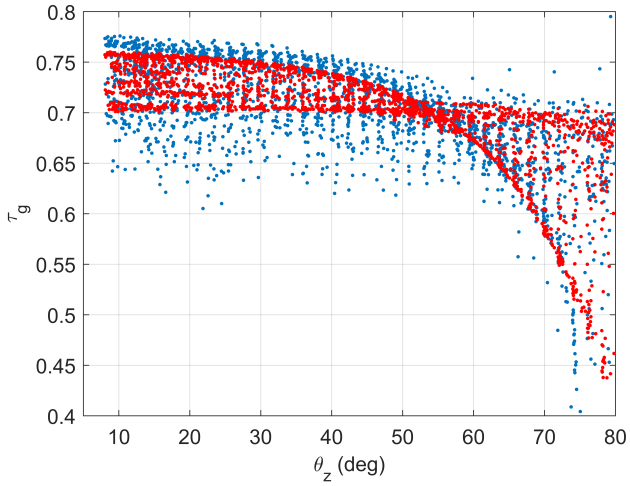

(b) Anisotropic model for horizontal case

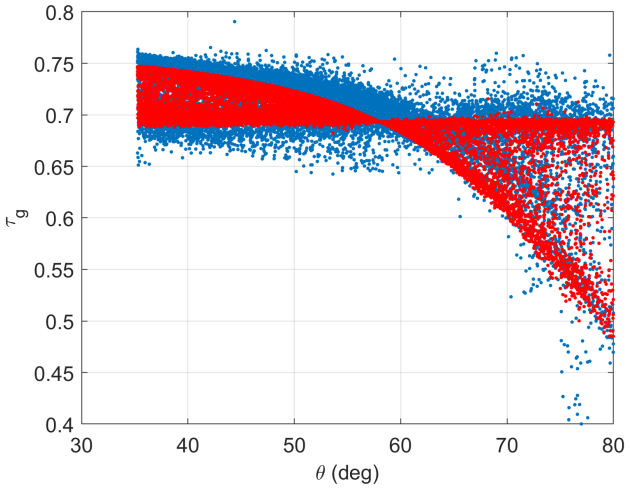

(c) Isotropic model for vertical case

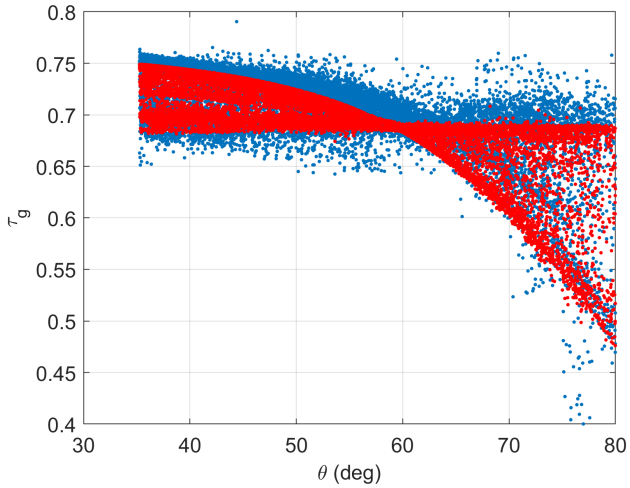

(d) Anisotropic model for vertical case

Figure 4: Transmittance measured (blue) vs modelled (red) for horizontal (a & b) and vertical (c & d) glazing, expressed as a percentage to the average experimental transmittance, $\bar{\tau}_g = 0.689$ (horizontal) and $\bar{\tau}_g = 0.702$ (vertical).

Conclusions

In this work, the global solar transmittance of a float glass was measured experimentally for different sky conditions and two different orientations, horizontal plane and vertical plane oriented towards the equator. These measurements were contrasted with two theoretical models which took as input parameters the refractive index, the extinction coefficient, and the thickness of the sample. Both models used the physical model proposed by Duffie and Beckman (2006) for direct solar transmittance. The difference between models lies in the treatment of diffuse solar irradiance, the first model assumes an isotropic distribution and the second the anisotropic distribution proposed by Brunger and Hooper (1993a).

When evaluating the performance of the models, it was found that the anisotropic presents very small improvements with respect to the isotropic one. When discriminating the indicators by sky condition, the main improvement of the anisotropic model with respect to the isotropic model occurs for clear and partially cloudy conditions. For cloudy conditions the isotropic model performs best. A simple combination of both models is the best performing under all-sky conditions. However, the difference with the isotropic model is small ($+3\,\%$) specially considering the typical uncertainty in the experimental data.

Weighting the performance indicators by the incident solar irradiance, the difference between the models increases considerably, going from $3-5$ % to $12-22$ %. For vertical glazings, the transmittance model is usually used with a transposition model to obtain the solar irradiance components on a vertical plane from those on the horizontal plane. When the Perez et al. (1990) transposition model is included in the calculation of the transmitted solar irradiance, the overall performance is degraded considerably and the advantage from using an anisotropic model is further reduced. Since, in all cases the performance indicators are of the same order of magnitude as the typical uncertainty of the measurements, a clear advantage for the anisotropic model can not be shown. Taking into account the balance between complexity, robustness (against data errors) and accuracy, the isotropic model continues to be the best option within the context of the BPSPs for most cases. However, for special applications which have large glazing/wall ratios and low Sun incidence angles during significant part of the day, may still benefit from including anisotropic effects in the diffuse component calculations.

Acknowledgment

References

Brandemuehl, M. and W. Beckman (1980). Transmission of diffuse radiation through cpc and flat plate collector glazings. *Solar Energy 24*(5), 511–513.

Brunger, A. P. and F. C. Hooper (1993a). Anisotropic sky radiance model based on narrow field of view measurements of shortwave radiance. *Solar Energy 51*(1), 53–64.

Brunger, A. P. and F. C. Hooper (1993b). Erratum to anisotropic sky radiance model based on narrow field of view measurements of shortwave radiance. *Solar Energy 51*(6), 523.

Duffie, J. and W. Beckman (2006). *Solar Engineering of Thermal Processes* (Third ed.). Hoboken, New Jersey: Wiley and Sons, Inc.

Gueymard, C. A. (2014). A review of validation methodologies and statistical performance indicators for modeled solar radiation data: Towards a better bankability of solar projects. *Renewable and Sustainable Energy Reviews 39*, 1024 – 1034.

Igawa, N., Y. Koga, T. Matsuzawa, and H. Nakamura (2004). Models of sky radiance distribution and sky luminance distribution. *Solar Energy 77*(2), 137–157.

World Meteorological Organization (WMO) (2005). *Baseline Surface Radiation Network (BSRN) Operations Manual*. www.wmo.org.

Moon, P. and D. Spencer (1942). Illumination from a non-uniform sky. *Illum. Engng.(NY) 37*, 707–726.

Perez, R., P. Ineichen, R. Seals, J. Michalsky, and R. Stewart (1990). Modeling daylight availability and irradiance components from direct and global irradiance. *Solar Energy 44*(5), 271 – 289.

Rodríguez-Muñoz, J., A. Monetta, R. Alonso-Suárez, I. Bove, and G. Abal (2021). Correction methods for shadow-band diffuse irradiance measurements: assessing the impact of local adaptation. *Renewable Energy 178*, 830–844.

Vitale, G., G. Abal, I. Bove, and J. Pereyra (2019). Global solar transmittance of vertical glazings. In *ISES Solar World Congress 2019 Proceedings*, pp. 1837 – 1847.

Wilbert, S., N. Geuder, M. Schwandt, B. Kraas, W. Jessen, R. Meyer, and B. Nouri (2015). Best practices for solar irradiance measurements with rotating shadowband irradiometers. *Solar Resource Assessment and Forecasting 178*, 25–26.

Yang, D. (2016). Solar radiation on inclined surfaces: Corrections and benchmarks. *Solar Energy 136*, 288–302.